

# Polarity tuning of spin-orbit-induced spin splitting in two-dimensional transition metal dichalcogenides semiconductors

Moh. Adhib Ulil Absor,\* Iman Santosa, Harsojo, and Kamsul Abraha

*Department of Physics, Universitas Gadjah Mada BLS 21 Yogyakarta Indonesia.*

Hiroki Kotaka

*Elements Strategy Initiative for Catalysts and Batteries (ESICB), Kyoto University, Kyoto 615-8520, Japan*

Fumiyuki Ishii and Mineo Saito

*Faculty of Mathematics and Physics Institute of Science and Engineering Kanazawa University 920-1192 Kanazawa Japan.*

(Dated: July 22, 2022)

The established spin splitting in monolayer (ML) of transition metal dichalcogenides (TMDs) that is caused by inversion symmetry breaking is dictated by mirror symmetry operations to exhibit fully out-of-plane direction of spin polarization. Through first-principles density functional theory calculations, we show that polarity-induced mirror symmetry breaking leads to new sizable spin splitting having in-plane spin polarization. These splittings are effectively controlled by tuning the polarity using biaxial strain. Furthermore, the admixtures of the out-of-plane and in-plane spin-polarized states in the strained polar systems are identified, which is expected to influence the spin relaxation through the Dyakonov-Perel mechanism. Our study clarified that the polarity-induced mirror symmetry breaking plays an important role in controlling the spin splitting and spin relaxation in the TMDs ML, which is useful for designing future spintronic devices.

## I. INTRODUCTION

Spin-orbit-coupled systems, which play a significant role in spintronics device operations, have attracted considerable scientific interest over recent years. This spin-orbit coupling (SOC) allows for the manipulation of electron spin<sup>1</sup>, leading to the interesting effect such as current-induced spin polarization<sup>2</sup>, the Spin Hall Effect<sup>3</sup>, the spin galvanic-effect<sup>4</sup>, and the spin ballistic transport<sup>5</sup>. For spintronics device operation, semiconducting structures are promising because of their manipulability under gate voltages<sup>6,7</sup>. However, a stable two-dimensional (2D) thin films with sufficiently large SOC are highly desirable for circuit integration. Here, the attentions are given for the polar semiconductor BiTeI, where large SOC has been reported<sup>8</sup>. In such material, the strong SOC is originated from their layer configuration, which is similar to 2D electron gas. However, due to the ionic bonding between layers, indicating that a stable free-standing film is not easy to be achieved. On the other hand, some attentions are also addressed to the stable 2D materials, which is focused on the carbon systems such as graphene<sup>9</sup> and their analogs such as silicene and germanene<sup>10</sup>, due to their exotic properties such as high carrier mobility and long spin lifetime<sup>11–13</sup>. However, the weak SOC effect in such materials<sup>11,12</sup> may limit their functionality for spintronic applications.

Recently, monolayer (ML) of transition metal dichalcogenides (TMDs) systems, a new class of the 2D materials, has attracted much attention because of their extraordinary properties such as the exotic spin-valley

coupled electronic structures that promise future spintronic and valleytronic applications<sup>14–21</sup>. The bulk phase of the TMDs systems is characterized by an inversion symmetric of  $2H\ MX_2$  stacking orders with space group  $D_{6h}$ <sup>22</sup>. However, in the ML phase, inversion symmetry is broken, leading to the fact the symmetry reduces to be  $D_{3h}$ <sup>17,20</sup>. Due to the inversion symmetry breaking together with strong spin-orbit coupling (SOC) in the  $5d$  orbitals of transition metals atoms, large spin splitting is established in the  $MX_2$  ML<sup>16,17,19,20,23</sup>, which plays an important role in inducing some of interesting phenomena such as spin Hall effect<sup>24,25</sup>, spin- and valley-dependent selection rule for optical transitions<sup>21</sup>, and magnetoelectric effect<sup>26</sup>. However, additional mirror symmetry operations in the  $MX_2$  TMDs ML suppresses the spin splitting to exhibit fully out-of-plane spin polarization, which is believed to be responsible for inducing strongly enhanced spin relaxation through Dyakonov-Perel mechanism<sup>17,20,27,28</sup>. Previous experimental studies have confirmed that long-lived spin relaxation and spin coherence of electrons have been reported on various  $MX_2$  ML such as MoS<sub>2</sub> ML<sup>27,28</sup> and WS<sub>2</sub> ML<sup>28</sup>.

Because the mirror symmetry plays a significant role in controlling the spin splitting and spin-polarized states in the  $MX_2$  ML, new electronic properties are expected to appear by breaking the mirror symmetry. Such situation is achieved by introducing the polar structures  $MXY$ <sup>29,30</sup>, in which the polarity that is originated from out-of-plane distance different between transition metal ( $M$ ) and chalcogen ( $X,Y$ ) atoms breaks the mirror symmetry. Experimentally, it is possible to create

such polar structures by growth on the polar substrate by recently developed molecular beam epitaxial (MBE) technique<sup>31,32</sup>. This supported by the fact that the stability of various polar  $MXY$  structures such as WSe and MoSSe has been reported<sup>29,30</sup>. However, due to the structural-dependent of the polarity, controlled changes in the polar structure, for example by applying strain, effectively tunes the polarity, which is expected to induce new useful properties for spintronics.

In this paper, we perform fully-relativistic first-principles density functional calculations to clarify the polarity-strain dependent on the electronic properties of the TMDs ML. We find that in addition to the established spin splitting having fully-out-of-plane spin polarization, a new sizable spin splitting exhibiting in-plane spin polarization is observed in the polar  $MXY$  ML. These splittings are found to be effectively controlled by tuning the polarity, which is achieved by applying biaxial strain. The origin of the spin splitting and spin-polarized states is analyzed on the basis of symmetry arguments combined with orbital hybridization analyses. Furthermore, the admixtures of the out-of-plane and in-plane spin-polarized states in the strained polar systems are identified, and their implication to the spin relaxation is discussed. Finally, the possible applications of our systems for spintronics are discussed.

## II. COMPUTATIONAL METHODS

Similar to the case of the non-polar  $MX_2$  systems, crystal structures of the polar  $MXY$  systems consists of  $X-M-Y$  slabs weakly bonded by van der Waals interaction<sup>22</sup>. Here, hexagonally layers of the transition metal atoms ( $M$ ) is sandwiched between two layers of the chalcogenide atoms ( $X,Y$ ) through strong ionic-covalent bonds forming a trigonal prismatic arrangement. In the case of the non-polar  $MX_2$  systems, its bulk structure shows an inversion symmetric of a  $2H$  stacking order with a space group of  $D_{6h}$  [Fig. 1(a)], while its monolayer (ML) structure has inversion symmetry breaking, which is together with the mirror symmetry of the  $X-M-X$  slab [Fig. 1(b)], make the symmetry reduces to be  $D_{3h}$ <sup>17,20</sup>. On the contrary, in the case of polar  $MXY$  ML, both inversion symmetry and mirror symmetry are broken, resulting in that the crystal symmetry becomes  $C_{3v}$ <sup>29</sup>. Because the physics in the polar  $MXY$  and non-polar  $MX_2$  ML systems are essentially the same for the group- VI transition metal dichalcogenides (TMDs), we here choose WSe and  $WS_2$  MLs as an example of the polar  $MXY$  and non-polar  $MX_2$  MLs, respectively.

We performed first-principles electronic structure calculations based on the density functional theory (DFT) within the generalized gradient approximation (GGA)<sup>33</sup> using the OpenMX code<sup>34</sup>. We used norm-conserving pseudopotentials<sup>35</sup>, and the wave functions are expanded by the linear combination of multiple pseudoatomic orbitals (LCPAOs) generated using a confine-

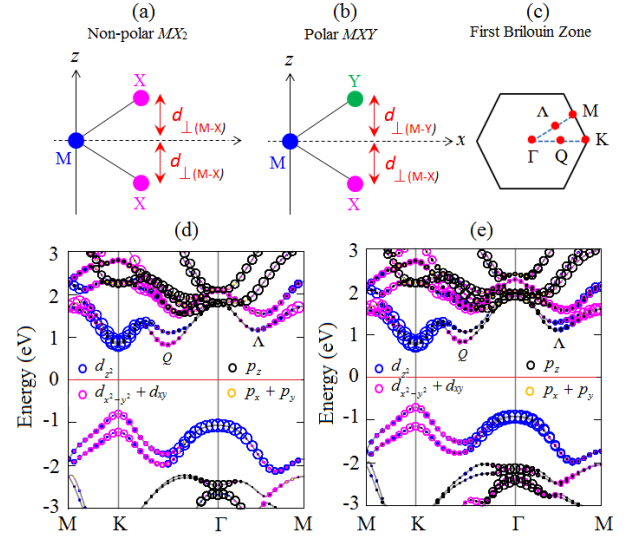


FIG. 1. Side view of (a) the non-polar  $MX_2$  and (b) the polar  $MXY$  monolayers (MLs) structures. These structures are characterized by the out-of-plane distance between transition metal ( $M$ ) and chalcogen atoms ( $X,Y$ ) [ $d_{\perp(M-Y)}$ ,  $d_{\perp(M-X)}$ ]. In the case of the non-polar  $MX_2$ , the mirror symmetry operation on the hexagonal plane is identified, while the mirror symmetry is broken in the case of polar  $MXY$  ML due to out-of-plane asymmetric of the structures. (c) First Brillouin zone, which is specified by the high symmetry points ( $\Gamma$ ,  $K$ , and  $M$  points) is shown. Here, new special points located along the  $\Gamma$ - $K$  line, namely the  $Q$  point, and along the  $\Gamma$ - $M$  line, namely the  $\Lambda$  point are indicated. Orbital-resolved of the electronic band structures for (c) the non-polar  $WS_2$  ML and (d) the polar  $WSe$  ML. The radius of circles reflects the magnitudes of spectral weight of the particular orbitals to the band.

ment scheme<sup>36,37</sup>. The orbitals are specified by  $W7.0-s^2p^2d^2f^1$ ,  $S9.0-s^2p^2d^1$ , and  $Se9.0-s^2p^2d^1$ , which means that the cutoff radii are 7.0, 9.0, and 9.0 bohr for the W, S, and Se atoms, respectively, in the confinement scheme<sup>36,37</sup>. For the W atoms, two primitive orbitals expand the  $s$ ,  $p$ , and  $d$  orbitals, and one primitive orbital expands the  $f$  orbital. On the other hand, for the S and Se atoms, two primitive orbitals expand the  $s$  and  $p$  orbitals, and one primitive orbital expands  $d$  orbital. Spin-orbit coupling (SOC) was included in our fully relativistic calculations, and the spin textures in  $k$ -space were calculated using the  $k$ -space spin density matrix of the spinor wave function<sup>20,38-41</sup>.

Two-dimensional structures of the polar  $MXY$  ML are modeled as a periodic slab [Figs. 1(a)-1(b)] with a sufficiently large vacuum layer (25 Å) to avoid interaction between adjacent layers. The geometries were fully relaxed until the force acting on each atom was less than one meV/Å. Here, we find that the optimized in-plane lattice constant is 3.24 Å for the case of the polar  $WSe$  ML, which is larger than that of the non-polar  $WS_2$  ML (3.18 Å), but it is in a good agreement with previous result [3.24 Å<sup>29</sup> to 3.25 Å<sup>30</sup>]. Furthermore, we charac-

terize the degree of the polarity in our system by using out-of-plane interlayer distance difference,  $\Delta d_{\perp}$ , defined as  $\Delta d_{\perp} = |d_{\perp(M-Y)} - d_{\perp(M-X)}|$ , where  $d_{\perp(M-X)}$  and  $d_{\perp(M-Y)}$  are the distance between transition metal (M) atoms and chalcogen (X,Y) atoms in the out-of-plane direction. In the case of the non-polar WS<sub>2</sub> ML, we find that the calculated value of  $\Delta d_{\perp}$  is zero, indicating that this structure is symmetric, thus, justifying the non-polarity of this structures. On the other hand, in the case of the polar WSSe ML, it is found that the calculated value of  $\Delta d_{\perp}$  is 0.154 Å, showing that this system is polar. Because the value of  $\Delta d_{\perp}$  sensitively depends on the distance between transition metal (M) and chalcogen (X,Y) atoms in the out-of-plane direction, it is expected that the polarity of the present system can be controlled by applying strain.

### III. RESULT AND DISCUSSION

To investigate the effect of the polarity on the electronic properties of TMDs ML, we show in Figs. 1(d) and 1(e) orbital-resolved of electronic band structures calculated on the first Brillouin zone [Fig. 1(c)]. In the case of the non-polar WS<sub>2</sub> ML, we observed two local maxima in the valence band maximum (VBM) located on the *K* and  $\Gamma$  points, which are predominately filled by  $d_{x^2-y^2} + d_{xy}$  and  $d_{z^2}$  orbitals, respectively [Fig. 1(d)]. On the other hand, in the conduction band minimum (CBM), we identify two local minima with close in energy located on the *K* point and midway between the  $\Gamma$  and *K* points, namely the *Q* points, and one additional local minima with higher in energy located between the  $\Gamma$  and *M* points, namely the  $\Lambda$  point. Here, the *Q* and *K* points are mainly originated from the  $d_{x^2-y^2} + d_{xy}$  and  $d_{z^2}$  orbitals, respectively, while the  $\Lambda$  point is characterized by the mixed states between the  $d_{x^2-y^2} + d_{xy}$  and  $d_{z^2}$  orbitals [Fig. 1(d)]. Since the VBM and CBM are centered at the *K* point in the non-polar WS<sub>2</sub> ML, a direct band gap with an energy gap of 1.68 eV is achieved, which is in good agreement with former calculation<sup>20,42</sup>. These features of electronic band structures are consistent with the recent observation of the electronic properties across the non-polar ML TMDs family<sup>17-20</sup>.

Similarly, the direct band gap is also observed in the case of the polar WSSe ML [Fig. 1(e)]. However, the energy gap is found to be 1.55 eV, which is smaller than that of the non-polar WS<sub>2</sub> ML. In the WSSe ML, out-of-plane crystal asymmetry enhances hybridization between out-of-plane orbitals [ $d_{z^2}$ ,  $p_z$ ], leading to the fact that energy level of the *K* point in the CBM shifts to be lower than that observed on the non-polar WS<sub>2</sub> ML, thus induces lowering the band gap. By the same reason, the energy level of the  $\Lambda$  point shifts down to be closer to that of the *K* and *Q* points in the CBM [Fig. 1(e)]. As a consequent, new spin- and valley-dependent selection rule for optical transitions involving the *K*, *Q*, and  $\Lambda$  points in the CBM is expected to be observed, which

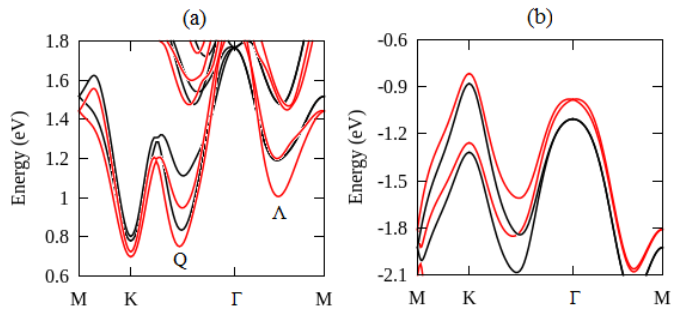


FIG. 2. Comparison of the electronic band structures between the non-polar WS<sub>2</sub> ML (black lines) and the polar WSSe ML (red lines) calculated (a) on the CBM and (b) VBM is shown.

is strongly different from that observed on the various non-polar TMDs ML<sup>21</sup>.

Turning the SOC, a spin splitting in the electronic band structures is established in both the non-polar and polar TMDs ML [Figs. 2(a)-2(b)] due to the absence of inversion symmetry. In the case of the non-polar WS<sub>2</sub> ML, the mirror symmetry operations suppresses the spin splitting to appear only along the  $\Gamma$ -*K* line. We find that large spin splitting up to 0.43 eV is observed at the *K* point in the VBM, while it is substantially small (0.03 eV) at the *K* point in the CBM. Here, we argue that different orbitals contribution at the *K* point between the CBM and VBM is responsible for inducing different magnitude of the spin splitting<sup>20</sup>. Moreover, the spin splitting of 0.33 eV is identified at the *Q* point in the CBM, which is lower than that at the *K* point in the VBM. Overall, the observed spin splittings in our calculational results are in a good agreement with recently reported data [ $\Delta E_{K,VBM}=0.426$  to  $0.433$  eV<sup>17-20</sup>;  $\Delta E_{Q,CBM}=0.2$  to  $0.33$  eV<sup>20,43</sup>;  $\Delta E_{K,CBM}=0.03$  eV<sup>20,23,43</sup>].

On the contrary, in the case of the polar WSSe ML, in addition to the observed spin splitting along the  $\Gamma$ -*K*, the SOC leads to a new sizable spin splitting along the  $\Gamma$ -*M* line due to the mirror symmetry breaking [see red colour lines in Figs. 2(a)-2(b)]. However, time reversal symmetry requires degenerated states at the  $\Gamma$  point, inducing Rashba type splitting around the  $\Gamma$  point, which is consistent with that previously reported by Cheng *et al.*<sup>29</sup>. We identify the large spin splitting of 0.48 eV at the *K* point in the VBM, which is comparable with that observed on the non-polar WS<sub>2</sub> ML. A comparable spin splitting is also observed at the *K* point in the CBM ( $\Delta E_{K,CBM} = 0.04$  eV). However, the spin splitting of 0.20 eV is observed at the *Q* point in the CBM, which is smaller than that observed on the non-polar WS<sub>2</sub> ML. Interestingly, we find new sizable spin splitting at the  $\Lambda$  point in the CBM,  $\Delta E_{\Lambda,CBM} = 0.22$  eV, which is comparable with that at the *Q* point. Because the energy level of  $\Lambda$  point is close to that of the *K* and *Q* point in the CBM, new spin conserving scattering processes involving the spin splitting at the *K*, *Q* and  $\Lambda$  points may occur, which is expected to induce new useful for spintronics.

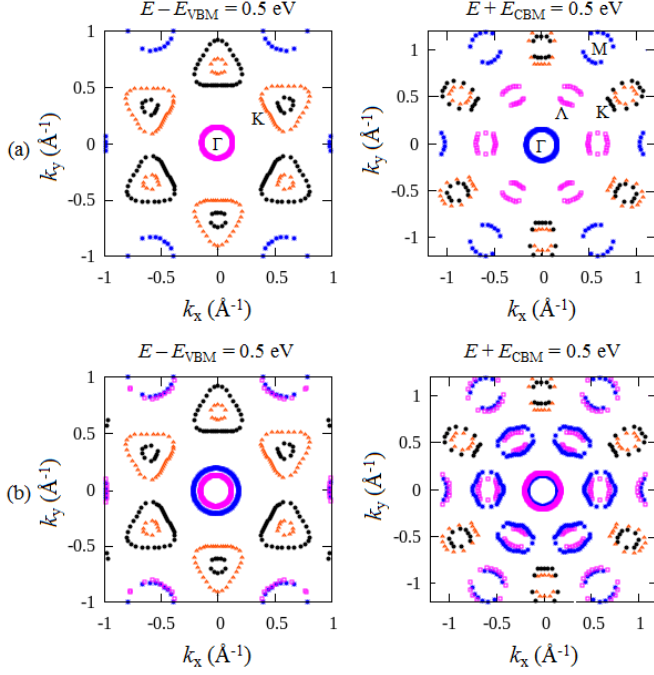


FIG. 3. The spin textures for (a) the non-polar  $\text{WS}_2$  ML and (b) polar  $\text{WSe}$  ML, which is calculated on the constant energy located on 0.5 eV below the VBM (left) and 0.5 above the CBM (right). The position of  $\Gamma$ ,  $K$ ,  $Q$ ,  $M$ , and  $\Lambda$  points are indicated. Here, black and red points represent out-of-plane spin polarization with up and down orientations, respectively, while pink and blue points show in-plane spin polarizations with clockwise and anti-clockwise orientations, respectively.

To further clarify the effect of the polarity on the observed spin splitting in our calculational results, we here calculate spin textures of the spin-split bands. Let us consider the spin textures, which is located on the 0.5 eV below the VBM. In the case of the non-polar  $\text{WS}_2$  ML, we find that the spin textures show six-fold symmetry of hole pockets, which is spin-split around the  $K$  point, but it is spin-degenerated around the  $\Gamma$  point [Fig. 3(a)]. Here, out-of-plane and in-plane spin polarizations characterize the spin-split hole pockets around the  $K$  point and the spin-degenerated hole pocket around the  $\Gamma$  point, respectively. However, the mirror symmetry breaking in the polar  $\text{WSe}$  ML lifts the degeneracy of the hole pockets around the  $\Gamma$  point, inducing a couple clockwise and anti-clockwise in-plane spin polarizations [Fig. 3(b)]. Consistently, the six-fold symmetry of the electron pockets is found at the energy of 0.5 eV above the CBM. Because of the polarity-induced symmetry breaking, electron pockets are spin-split, which appears along the  $\Gamma$ - $K$  and the  $\Gamma$ - $M$  lines. These spin-split electron pockets are characterized by the fully-out-of-plane and in-plane spin-polarized states along the  $\Gamma$ - $K$  and  $\Gamma$ - $M$  lines, respectively. The observed out-of-plane and in-plane spin-polarized states in our systems are expected to play a significant role in the spin-conserving scattering processes

that imply to the spin relaxation and intervalley scattering times<sup>27,28</sup>.

The origin of the observed spin splitting and the spin-polarized states in our calculational results can be understood in term of the symmetry arguments. The non-polar  $\text{WS}_2$  ML belongs to the symmetry point group of  $D_{3h}$ . This symmetry itself combines the  $C_{3v}$  symmetry group and a mirror reflection on the hexagonal plane of the first Brillouin zone [Fig. 1(a)]. However, in the case of the polar  $\text{WSe}$  ML, the polarity induces mirror symmetry breaking [Fig. 1(b)], leading to the fact that the symmetry reduces become  $C_{3v}$ . In this case, the SOI Hamiltonian up to cubic  $k$ -terms can be expressed as<sup>16,17,20,44–46</sup>

$$H(k) = \alpha_R(k_x\sigma_y - k_y\sigma_x) + \beta_k(3k_x^2 - k_y^2)k_y\sigma_z, \quad (1)$$

where  $k = \sqrt{k_x^2 + k_y^2}$  and  $\sigma_i$  are Pauli matrices. Here, the first term in the  $H(k)$  is the Rashba term characterized by Rashba parameter,  $\alpha_R$ , inducing in-plane components of spin polarizations. On the other hand, the second term in the  $H(k)$  is the warping term characterized by warping parameter,  $\beta_k$ , which contributes to the out-of-plane component of spin polarization. It is noted here that the Rashba parameter  $\alpha_R$  is induced by out-of-plane potential gradient asymmetry, while the warping parameter  $\beta_k$  is mainly contributed from in-plane potential gradient asymmetry<sup>17,44</sup>. By using the SOI Hamiltonian of the  $C_{3v}$  point group symmetry given in Eqs. (1), we find that the spin splitting bands can be expressed as<sup>44</sup>

$$\Delta E(k, \theta) = (\alpha_R^2 + \beta_k^2 \sin^2(3\theta))^{1/2}, \quad (2)$$

with the spin polarization vector,

$$P_{\pm}(k, \theta) = \pm[\alpha_R \sin \theta, -\alpha_R \cos \theta, -\beta_k \sin(3\theta)], \quad (3)$$

where  $\theta = \tan^{-1}(k_y/k_x)$ . The subscripts  $+$  and  $-$  denote spin-split states for the upper and lower bands, respectively.

In the case of the non-polar  $\text{WS}_2$  ML, the mirror symmetry operation of  $D_{3h}$  point group suppresses the Rashba term in the  $H(k)$ , leading to the fact that only the second term in the Eq. (2) remains. As a result, zero spin splitting is observed at  $\theta = n\pi/3$ , where  $n$  is an integer number, which is consistent with the observed spin degeneracy in the band structures along the  $\Gamma$ - $M$  line shown in Figs. 2(a) and 2(b). Furthermore, due to the last term of the Eq. (3), fully-out-of plane spin polarization is visible at  $\theta = (2n+1)\pi/6$ . This is, in fact, consistent with our calculated results of the spin textures along the  $\Gamma$ - $K$  line [Fig. 3(a)]. However, in the case of the polar  $\text{WSe}$  ML, the spin degeneracy along the  $\Gamma$ - $M$  line is broken [Figs. 2(a)-2(b)], which is due to the first term of the Eq. (2). Here, the spin-splitting bands have in-plane spin polarization due to the first term of Eq. (3), which is confirmed by our results shown in Fig. 3(b). Therefore, it can be concluded that the splitting



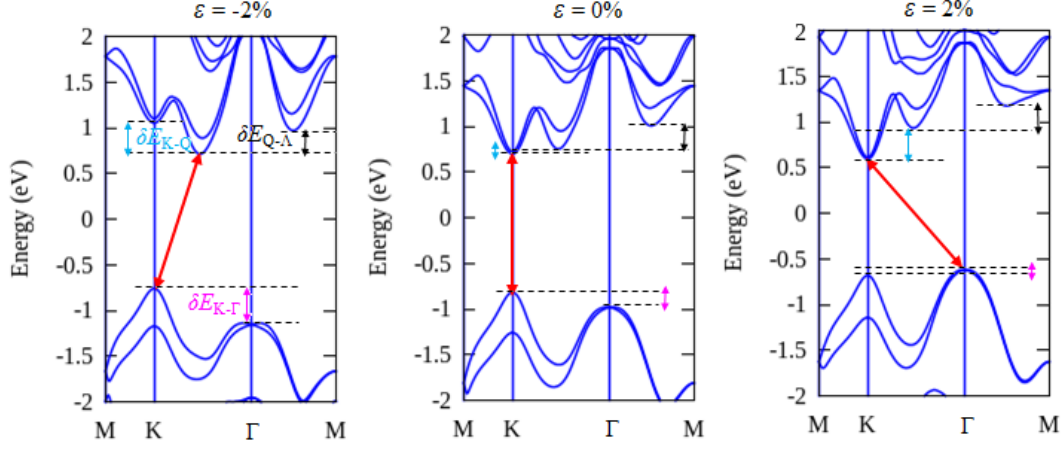


FIG. 4. Electronic band structures of the strained polar WSe<sub>2</sub> ML with  $\epsilon = -2\%$  (left),  $\epsilon = 0\%$  (center), and  $\epsilon = 2\%$  (right) are given. The red, pink, blue, and black arrows indicate the band gap, energy different between the  $K$  and  $\Gamma$  points ( $\delta E_{K-\Gamma}$ ), energy different between the  $K$  and  $Q$  points ( $\delta E_{K-Q}$ ), and energy different between the  $Q$  and  $\Lambda$  points ( $\delta E_{Q-\Lambda}$ ), respectively.

and spin textures in our calculational results are consistent well with the simplified Hamiltonian.

Because the polarity plays a significant role in the spin splitting properties of the TMDs ML, controlling the polarity is expected to induce new useful properties for spintronics. Here, the strain is an effective method to tune the polarity, which is achieved by applying substrates or doping effects<sup>31,32,47</sup>. To this aim, we use a wide range of biaxial strains (up to 8%) in the polar WSe<sub>2</sub> ML by tuning the planar lattice parameter. The range of strain considered here was chosen because the symmetry breaking of the crystal may occur for the larger strain. For an instant, in the MoS<sub>2</sub> ML such symmetry breaking is observed at an effective strain of 6 to 11 %<sup>48</sup>. We define the degree of in-plane biaxial strain as  $\epsilon = (a - a_0)/a_0$ , where  $a_0$  is the unstrained in-plane lattice constant. Here, we studied the following two different cases: the tensile strain, which increases the in-plane lattice constant  $a$ , and compressive strain, which decreases  $a$ .

Under the tensile strain, the interlayer distance difference between transition metal and chalcogen atoms in the out-of-plane direction  $\Delta d_{\perp}$  is decreased [Fig. 5(a)], and, consequently, the hybridization between the out-of-plane bonding states ( $d_{z^2}$ ,  $p_z$ ) is reduced, while the hybridization between the in-plane bonding states [ $d_{x^2-y^2} + d_{xy}$ ,  $S p_x + p_y$ ] is strengthened. The increased overlap of the in-plane bonding states with the tension can explain the decreased in energy of the  $K$  point with respect to that of the  $\Gamma$  point in the VBM [Fig. 4]. On the other hand, the compressive strain has the effect of shifting the energy level of the  $d_{x^2-y^2} + d_{xy}$  anti-bonding states to be lower than that of the  $d_{z^2}$  anti-bonding states, resulting in that the energy level of the  $Q$  point becomes lower than that of the  $K$  point in the CBM. Thus, strain sensitively controls the energy level at the high symmetry points in the VBM and CBM.

The shifted of energy level at the high symmetry points in the CBM and VBM by the strain has two important effects. The first is the appearance of the indirect band gap. Here, the optical transition from the  $K$  point in the CBM to the  $\Gamma$  point in the VBM is observed under the tensile strain, while it changes from the  $Q$  point in the CBM to the  $K$  points in the VBM when the compressive strain is introduced [Fig. 4]. It is pointed out here that transition from the direct to the indirect band gap is achieved on a substantial critical strain, which is observed on -0.25 % and 1.9 % for the compressive and tensile strains, respectively. These values are slightly different from that seen on the non-polar WS<sub>2</sub> ML [(-1.2 % and 2.3 %) <sup>20</sup>], but consistent with previous result reported by Defo *at. al.*<sup>30</sup>. The second effect is the changed of energy different between the high symmetry points in the CBM and VBM [Fig. 5(b)]. In the VBM, we find that the energy different between the  $K$  and  $\Gamma$  points,  $\delta E_{K-\Gamma}$ , enhances by increasing the compressive and tensile strains [Fig. 5(b)]. Similarly, the increased of energy different between the  $K$  and  $Q$  points,  $\delta E_{K-Q}$ , and between the  $Q$  and  $\Lambda$  points,  $\delta E_{Q-\Lambda}$  in the CBM is also identified. Remarkably, tuning the polarity by the strain strongly modifies the electronic properties of the polar WSe<sub>2</sub> ML.

The strong modification of the electronic properties by the strain is expected to significantly change the spin splitting properties of the polar WSe<sub>2</sub> ML. In the VBM, the increased overlap of the in-plane bonding states [ $d_{x^2-y^2} + d_{xy}$ ,  $S p_x + p_y$ ] by the tensile strain leads to substantial enhancement of the spin splitting at the  $K$  point, while it decreases the spin splitting around the  $\Gamma$  point [Fig. 5(c)]. On the contrary, introducing the compressive strain increases the overlap of the out-of-plane bonding states ( $d_{z^2}$ ,  $p_z$ ), leading to the fact that the spin splitting around the  $\Gamma$  point enlarges but it contributes only small to the spin splitting at the  $K$  point. We also

find the strong enhancement of the spin splitting in the CBM, which is observed at the  $Q$  and  $\Lambda$  points under the tensile strain, and at the  $K$  point under the compressive strain. Therefore, the application of the strain sensitively tunes the spin-splitting in the CBM and VBM of the polar WSSe ML, which is expected to be useful for spintronics applications.

Before continuing our discussion on possible spintronic applications of the enhanced spin splitting in the strained polar WSSe ML, we briefly comment on the seemingly spin splitting features around the  $\Gamma$  point in the VBM known as the Rashba splitting [see Fig. 4]. A comprehensive discussion of the Rashba splitting in the TMDs ML has been previously presented by Cheng *et al.*<sup>29</sup>. However, they have not considered the effect of the strain, which motivated us to extend their study. Naturally, the non-zero of  $\Delta d_{\perp}$  induces asymmetry of potential gradient perpendicular to the surface plane, leading to the strong hybridization between the out-of-plane bonding states [ $d_{z^2}$ ,  $p_z$ ] in the  $\Gamma$  point. Consequently, the SOC leads to the substantial spin splitting except for the  $\Gamma$  point due to time reversibility. However, decreasing (increasing)  $\Delta d_{\perp}$  by the compressive (tensile) strains [Fig. 5(a)], subsequently reduces (strengthens) the coupling between the out-of-plane bonding states, thus decreasing (increasing) the Rashba splitting. The considerable changes of the Rashba splitting by the strain is, in fact, consistent with the modulation of the Rashba parameter  $\alpha_R$  shown in Fig. 5(d). The observed Rashba splitting in our calculational results supports the recent prediction of the Rashba splitting on strained MoS<sub>2</sub>/Bi(111) heterostructures<sup>49</sup>, where the broken mirror symmetry by the substrates plays an important role in generating the Rashba splitting in the various TMDs ML.

From the application point of view, the enhanced spin-splitting in the VBM and CBM indicates that  $p$ - and  $n$ -type systems are promising for spintronics. In the case of the unstrained system, both the VBM and CBM are located on the  $K$  point [Fig. 4(b)]. However, the spin splitting in the VBM ( $\Delta E_{K-\text{VBM}} = 0.48$  eV) is much larger than that in the CBM ( $\Delta E_{K-\text{CBM}} = 0.03$  eV), thus,  $p$ -type system is more suitable for spintronics. Since the energy different between the  $K$  and  $\Gamma$  points in the VBM is large ( $\delta E_{K-\Gamma} = 0.48$  eV), weak admixtures of states are expected to be achieved. Accordingly, transport hole carriers should rely on states close to the  $K$  point. Under the compressive strain, the VBM and CBM are located on the  $K$  and  $Q$  points, respectively, exhibiting the large spin splitting. For instant, at -2% compressive strain, we found that  $\Delta E_{K-\text{VBM}} = 0.45$  eV at the  $K$  point in the VBM and  $\Delta E_{Q-\text{CBM}} = 0.21$  eV at the  $Q$  point in the CBM, suggesting that both the  $p$ - and  $n$ -type compressively strained systems are suitable for spintronics. On the contrary, introducing the tensile strain leads to the small spin splitting in the VBM and CBM [Fig. 4(c)], which is not suitable for spintronics. The predicted  $n$ - and  $p$ -type systems can be achieved by introducing electron and hole dopings, respectively, which is similar to

those observed on the various non-polar TMDs ML<sup>47</sup>. As such, our findings of the tunable spin splitting are useful for realizing spintronics applications of the polar TMDs ML.

Here, we discuss other possible spintronic applications of the polar WSSe ML based on the features of the spin textures. In the case of the unstrained system, the substantially large of the energy different between  $K$  and  $\Gamma$  points,  $\delta E_{K-\Gamma}$ , in the VBM leads to the weak admixtures of states between the  $K$  and the  $\Gamma$  points. Because the energy level of the  $K$  point is much higher than that of the  $\Gamma$  point, the spin textures are dominated by the spin-split hole pockets around the  $K$  point exhibiting out-of-plane spin polarization [Fig. 3(b)]. These features of spin polarization are expected to induce spin-orbit fields perpendicular to the crystal plane,  $B_{SO\perp}$ , implying that unusually long spin lifetimes without intervalley scattering is achieved through the Dyakonov-Perel spin relaxation mechanism<sup>17,20</sup>. This is supported by the fact that a similar mechanism behind the long spin lifetimes induced by out-of-plane spin polarization has been reported on the various TMDs ML<sup>27,28,43</sup>, suggesting that the present system is promising for spintronics applications. Such situation is also achieved in the CBM since the fully out-of-plane spin polarized states are visible at the  $K$  and  $Q$  points. Because the energy level of the  $K$  and  $Q$  points is close, spin conserving scattering between the  $K$  and  $Q$  points may occur, which induces intervalley quantum interference that is similar to those observed on the WS<sub>2</sub> ML<sup>43</sup>.

Interestingly, the significant admixtures of states are expected to occur between the  $K$  and  $\Gamma$  points in the VBM under the small tensile strain due to the small  $\delta E_{K-\Gamma}$  [Fig. 5(b)]. Here, the coupling between out-of-plane spin-orbit fields  $B_{SO\perp}$  around the  $K$  point and in-plane spin-orbit fields  $B_{SO\parallel}$  around the  $\Gamma$  point is strengthened. However, due to the substantially small spin splitting around the  $\Gamma$  point, weak in-plane spin-orbit field  $B_{SO\parallel}$  is generated, which induces small misalignment of the total spin-orbit fields from the out-of-plane direction, implying that the spin relaxation times becomes much longer than that intervalley scattering times. This situation is qualitatively similar to the recent observation of the spin lifetimes on dual gated exfoliated MoS<sub>2</sub> ML reported by Schmidt *et al.*<sup>27</sup>, which found that applying ionic gating breaks the mirror symmetry to induces the enhanced spin relaxation. On the other hand, the observed small  $\delta E_{Q-\Lambda}$  under the compressive strain leads to the significant admixtures of states between the  $Q$  and  $\Lambda$  points in the CBM, inducing strong coupling between the  $B_{SO\perp}$  and  $B_{SO\parallel}$  in the  $Q$  and  $\Lambda$  points, respectively. Because the strength between the  $B_{SO\perp}$  and  $B_{SO\parallel}$  is comparable due to the comparable spin splitting between the  $Q$  and  $\Lambda$  points [Fig. 5(c)], a strong intervalley scattering is achieved, which implies to the decreasing of the spin relaxation times. Therefore, our study clarifies that the polarity-induced mirror symmetry breaking in the TMDs ML is an effective way to controlling the

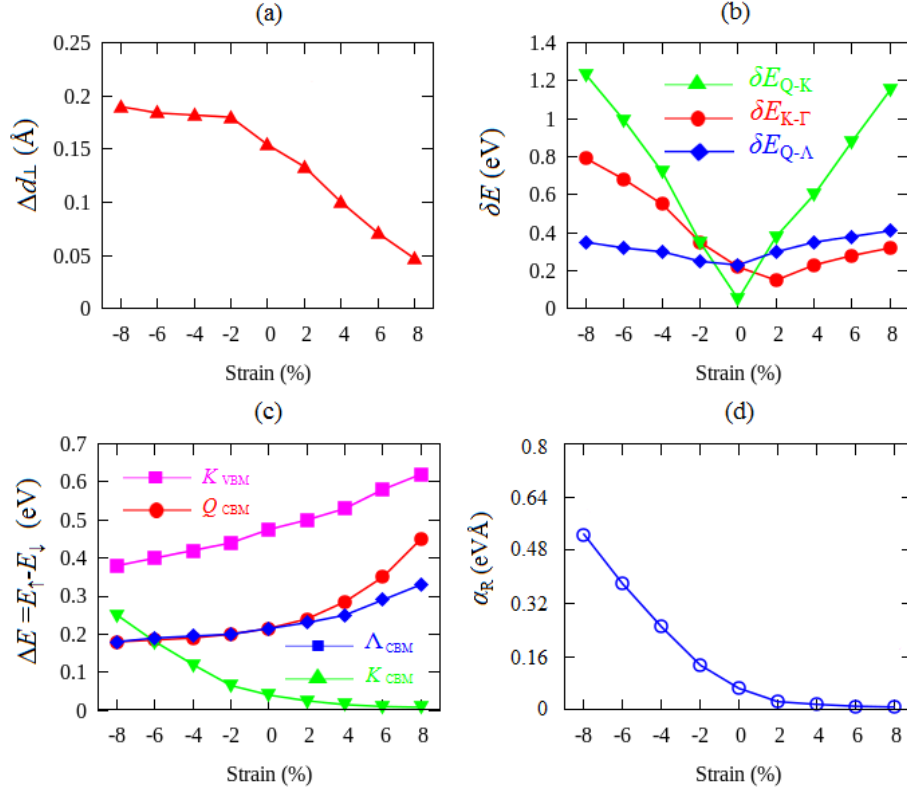


FIG. 5. (a) Strain-dependent of the out-of-plane interlayer distance difference ( $\Delta d_{\perp}$ ) in the polar WSe ML is shown. (b) The calculated energy different  $\delta E$  between the high symmetry points in the CBM and VBM as a function of strain. (c) Strain-dependent of the absolute spin splitting energy  $\Delta E = |E_{\uparrow} - E_{\downarrow}|$  at the high symmetry points in the CBM and VBM. (d) The Rashba parameter ( $\alpha_R$ ) as a function of strain, calculated around the  $\Gamma$  point in the VBM.

spin relaxation, which is useful for designing future spintronics devices.

It is to be noted that our proposed approach for generating and modulating the spin splitting and spin-polarized states is not limited to the polar WSe ML, but it can be generalized to a variety of SOC systems with the polar  $MXY$  structures exhibiting the polarity-induced mirror symmetry breaking (for example, other the polar TMDs ML including WSTe, MoSSe and MoSTe whose electronic structure properties are similar to WSe ML<sup>29,30</sup>). Together, these features seem to be promising for inducing new electronic properties which are useful for spintronic applications.

#### IV. CONCLUSION

To summarize, we have investigated the effect of the polarity and its strain dependent on the electronic properties of the TMDs ML by using fully-relativistic first-principles density functional theory calculations. We found that in addition to the established spin splitting along the  $\Gamma$ - $K$  line with fully-out-of-plane spin polarization, the presence of the mirror symmetry breaking in the polar TMDs ML leads to new sizable spin split-

ting along the  $\Gamma$ - $M$  line exhibiting in-plane spin polarization. We also find that these splittings are effectively controlled by tuning the polarity realized by introducing biaxial strain. We clarified the origin of the spin splitting and spin polarization in our calculational results by using symmetry arguments combined with orbital hybridization analyses. The enhanced and sizable spin splittings found in the present study suggested that the strained polar TMDs ML systems are suitable for spintronic applications. Finally, we have identified the possible admixtures of the out-of-plane and in-plane spin-polarized states in the strained polar systems and discussed its implication to the spin relaxation involving intervalley scattering process through the Dyakonov-Perel mechanism. Our study clarified that the polarity-induced mirror symmetry breaking is an efficient way of controlling the spin splitting and spin relaxation times in the TMDs ML, which is useful for designing future spintronic devices.

#### ACKNOWLEDGMENTS

This work was partly supported by the Fundamental Research Grant (2017) funded by the ministry of research

and technology and higher education, Republic of Indonesia. Part of this research was supported by BOPTN research grant (2016) founded by Faculty of Mathematics and Natural Sciences, Universitas Gadjah Mada. The

computations in this research were performed using the high performance computing facilities (DSDI) at Universitas Gadjah Mada, Indonesia.

- 
- \* adib@ugm.ac.id
- <sup>1</sup> Y. Kato, R. C. Myers, A. C. Gossard, and D. D. Awschalom, *Nature* **427**, 50 (2004).
  - <sup>2</sup> S. Kuhlén, K. Schmalbuch, M. Hagedorn, P. Schlammes, M. Patt, M. Lepsa, G. Güntherodt, and B. Beschoten, *Phys. Rev. Lett.* **109**, 146603 (2012).
  - <sup>3</sup> X.-L. Qi, Y.-S. Wu, and S.-C. Zhang, *Phys. Rev. B* **74**, 085308 (2006).
  - <sup>4</sup> S. D. Ganichev, E. L. Ivchenko, V. V. Belkov, S. A. Tarasenko, M. Sollinger, D. Weiss, W. Wegscheider, and W. Prettl, *Nature* **417**, 153 (2002).
  - <sup>5</sup> J. P. Lu, J. B. Yau, S. P. Shukla, M. Shayegan, L. Wissinger, U. Rössler, and R. Winkler, *Phys. Rev. Lett.* **81**, 1282 (1998).
  - <sup>6</sup> S. Datta and B. Das, *Appl. Phys. Lett.* **56**, 665 (1990).
  - <sup>7</sup> J. Nitta, T. Akazaki, H. Takayanagi, and T. Enoki, *Phys. Rev. Lett.* **78**, 1335 (1997).
  - <sup>8</sup> K. Ishizaka, M. S. Bahramy, H. Murakawa, M. Sakano, T. Shimojima, T. Sonobe, K. Koizumi, S. Shin, H. Miyahara, A. Kimura, K. Miyamoto, T. Okuda, H. Namatame, M. Taniguchi, R. Arita, N. Nagaosa, K. Kobayashi, Y. Murakami, R. Kumai, Y. Kaneko, Y. Onose, and Y. Tokura, *Nat. Mater* **10**, 521 (2011).
  - <sup>9</sup> K. S. Novoselov, A. K. Geim, S. V. Morozov, D. Jiang, Y. Zhang, S. V. Dubonos, I. V. Grigorieva, and A. A. Firsov, *Science* **306**, 666 (2004).
  - <sup>10</sup> S. Cahangirov, M. Topsakal, E. Aktürk, H. Şahin, and S. Ciraci, *Phys. Rev. Lett.* **102**, 236804 (2009).
  - <sup>11</sup> H. Min, J. E. Hill, N. A. Sinitsyn, B. R. Sahu, L. Kleinman, and A. H. MacDonald, *Phys. Rev. B* **74**, 165310 (2006).
  - <sup>12</sup> C.-C. Liu, W. Feng, and Y. Yao, *Phys. Rev. Lett.* **107**, 076802 (2011).
  - <sup>13</sup> C. L. Kane and E. J. Mele, *Phys. Rev. Lett.* **95**, 226801 (2005).
  - <sup>14</sup> D. Xiao, G.-B. Liu, W. Feng, X. Xu, and W. Yao, *Phys. Rev. Lett.* **108**, 196802 (2012).
  - <sup>15</sup> X. D. Xu, W. Yao, D. Xiao, and T. F. Heinz, *Nat. Physics* **10**, 343 (2014).
  - <sup>16</sup> H. Yuan, M. S. Bahramy, K. Morimoto, S. Wu, K. Nomura, B.-J. Yang, H. Shimotani, R. Suzuki, M. Toh, C. Kloc, X. Xu, R. Arita, N. Nagaosa, and Y. Iwasa, *Nat. Physics* **9**, 563 (2013).
  - <sup>17</sup> Z. Y. Zhu, Y. C. Cheng, and U. Schwingenschlöggl, *Phys. Rev. B* **84**, 153402 (2011).
  - <sup>18</sup> D. W. Latzke, W. Zhang, A. Suslu, T.-R. Chang, H. Lin, H.-T. Jeng, S. Tongay, J. Wu, A. Bansil, and A. Lanzara, *Phys. Rev. B* **91**, 235202 (2015).
  - <sup>19</sup> G.-B. Liu, W.-Y. Shan, Y. Yao, W. Yao, and D. Xiao, *Phys. Rev. B* **88**, 085433 (2013).
  - <sup>20</sup> M. A. U. Absor, H. Kotaka, F. Ishii, and M. Saito, *Phys. Rev. B* **94**, 115131 (2016).
  - <sup>21</sup> R.-L. Chu, X. Li, S. Wu, Q. Niu, W. Yao, X. Xu, and C. Zhang, *Phys. Rev. B* **90**, 045427 (2014).
  - <sup>22</sup> R. A. Bromley, R. B. Murray, and A. D. Yoffe, *Journal of Physics C: Solid State Physics* **5**, 759 (1972).
  - <sup>23</sup> K. Kośmider, J. W. González, and J. Fernández-Rossier, *Phys. Rev. B* **88**, 245436 (2013).
  - <sup>24</sup> M. A. Cazalilla, H. Ochoa, and F. Guinea, *Phys. Rev. Lett.* **113**, 077201 (2014).
  - <sup>25</sup> Y. Ma, L. Kou, X. Li, Y. Dai, S. C. Smith, and T. Heine, *Phys. Rev. B* **92**, 085427 (2015).
  - <sup>26</sup> Z. Gong, G.-B. Liu, H. Yu, D. Xiao, X. Cui, X. Xu, and W. Yao, *Nat. Commun.* **4**, 2053 (2013).
  - <sup>27</sup> H. Schmidt, I. Yudhistira, L. Chu, A. H. Castro Neto, B. Özyilmaz, S. Adam, and G. Eda, *Phys. Rev. Lett.* **116**, 046803 (2016).
  - <sup>28</sup> L. Yang, N. A. Sinitsyn, W. Chen, J. Yuan, J. Zhang, J. Lou, and S. A. Crooker, *Nat. Physics* **11**, 830 (2015).
  - <sup>29</sup> Y. C. Cheng, Z. Y. Zhu, M. Tahir, and U. Schwingenschlöggl, *EPL* **102**, 57001 (2013).
  - <sup>30</sup> R. K. Deho, S. Fang, S. N. Shirodkar, G. A. Tritsarlis, A. Dimoulas, and E. Kaxiras, *Phys. Rev. B* **94**, 155310 (2016).
  - <sup>31</sup> E. Xenogiannopoulou, P. Tsipas, K. E. Aretouli, D. Tsoutsou, S. A. Giamini, C. Bazioti, G. P. Dimitrakopoulos, P. Komninou, S. Brems, C. Huyghebaert, I. P. Radu, and A. Dimoulas, *Nanoscale* **7**, 7896 (2015).
  - <sup>32</sup> K. E. Aretouli, P. Tsipas, D. Tsoutsou, J. Marquez-Velasco, E. Xenogiannopoulou, S. A. Giamini, E. Vassalou, N. Kelaidis, and A. Dimoulas, *Applied Physics Letters* **106**, 143105 (2015).
  - <sup>33</sup> J. P. Perdew, K. Burke, and M. Ernzerhof, *Phys. Rev. Lett.* **77**, 3865 (1996).
  - <sup>34</sup> T. Ozaki, H. Kino, J. Yu, M. J. Han, N. Kobayashi, M. Ohfuti, F. Ishii, T. Ohwaki, H. Weng, and K. Terakura, <http://www.openmx-square.org/>.
  - <sup>35</sup> N. Troullier and J. L. Martins, *Phys. Rev. B* **43**, 1993 (1991).
  - <sup>36</sup> T. Ozaki, *Phys. Rev. B* **67**, 155108 (2003).
  - <sup>37</sup> T. Ozaki and H. Kino, *Phys. Rev. B* **69**, 195113 (2004).
  - <sup>38</sup> H. Kotaka, F. Ishii, and M. Saito, *Jpn. J. Appl. Phys.* **52**, 035204 (2013).
  - <sup>39</sup> M. A. U. Absor, H. Kotaka, F. Ishii, and M. Saito, *Applied Physics Express* **7**, 053002 (2014).
  - <sup>40</sup> M. A. U. Absor, F. Ishii, H. Kotaka, and M. Saito, *Applied Physics Express* **8**, 073006 (2015).
  - <sup>41</sup> M. A. U. Absor, F. Ishii, H. Kotaka, and M. Saito, *AIP Advances* **6**, 025309 (2016).
  - <sup>42</sup> D. M. Guzman and A. Strachan, *Journal of Applied Physics* **115**, 243701 (2014).
  - <sup>43</sup> H. Liu, J. Chen, H. Yu, F. Yang, L. Jiao, G.-B. Liu, W. Ho, C. Gao, J. Jia, W. Yao, and M. Xie, *Nat. Commun* **6**, 8180 (2015).
  - <sup>44</sup> S. Vajna, E. Simon, A. Szilva, K. Palotas, B. Ujfalussy, and L. Szunyogh, *Phys. Rev. B* **85**, 075404 (2012).
  - <sup>45</sup> A. Kormányos, V. Zólyomi, N. D. Drummond, and G. Burkard, *Phys. Rev. X* **4**, 011034 (2014).
  - <sup>46</sup> A. Kormányos, G. Burkard, M. Gmitra, J. Fabian, V. Zlyomi, N. D. Drummond, and V. Falko, *2D Materials* **2**, 022001 (2015).



- <sup>47</sup> T. Brumme, M. Calandra, and F. Mauri, Phys. Rev. B **91**, 155436 (2015).
- <sup>48</sup> S. Bertolazzi, J. Brivio, and A. Kis, ACS Nano **5**, 9703 (2011), pMID: 22087740.
- <sup>49</sup> K. Lee, W. S. Yun, and J. D. Lee, Phys. Rev. B **91**, 125420 (2015).